PCCP

Accepted Manuscript

ROYAL SOCIETY OF CHEMISTRY

www.rsc.org/pccp

Journal Name

ARTICLE

D-A-D-Type Narrow-Bandgap Small-Molecule Photovoltaic Donors: Pre-Synthesis Virtual Screening by Density Functional Theory

Received 00th January 20xx,
Accepted 00th January 20xx

DOI: 10.1039/x0xx00000x

www.rsc.org/

Yeongrok Gim,[a] Daekyeom Kim,[a] Minkyu Kyeong,[a] Seunghwan Byun,[a] Yuri Park,[b] Sooncheol Kwon,[b] Heejoo Kim,[b] Sukwon Hong,[a,b,c,*] Yves Lansac,[d,*] and Yun Hee Jang[a,*]

A new series of D-A-D-type small-molecule photovoltaic donors are designed and virtually screened before synthesis by time-dependent density functional theory calculations carefully validated against various polymeric and molecular donors. In this series of new design, benzodithiophene is kept as D to achieve the optimum highest-occupied molecular orbital energy level, while thienopyrroledione is initially chosen as A but later replaced by difluorinated benzodiathiazole or its selenide derivative to achieve the optimum band gap. The D-A-D core is end-capped by pyridone units which could not only enhance their self-assembly via hydrogen bonds but also play a role as acceptor (A') to form an extended A'-D-A-D-A' small-molecule donor.

1. Introduction

An organic photovoltaic (OPV) cell made of low-cost light-weight flexible materials has a potential to bring the solar energy to various interesting applications. Its power conversion efficiency (PCE) has improved (<12%) with the introduction of a bulk heterojunction (BHJ) architecture where *push-pull* (or D-A) conjugated-copolymer donors (absorbing the solar spectrum in the near-IR region of 680-950 nm) form an interpenetrating network with fullerene-derivative acceptors. Narrow bandgap and high charge carrier mobility as well as efficient charge separation and collection are desirable for high-PCE OPV donors and often achieved via a morphology control.

Recently, OPV cells with small molecular donors have attracted a great deal of attention owing to their uniform and well-defined molecular structure circumventing batch-to-batch variations in molecular weight, polydispersity, and purity of polymeric donors.[1] A more reproducible morphology control and a finer energy-level control through chemical-structure modification could be achieved with small-molecule donors.[1]

They had received little attention due to their extremely low PCE (<1%) when first introduced in 2006,[2,3] but the PCE reached 6.7% with a D1-A-D2-A-D1 type of small-molecule donor DTS(PTTh$_2$)$_2$ in 2012,[1] and it has further improved up to 8-9% with a continuous optimization of the molecular structure which modifies or replaces each unit to introduce new A-D-A combinations.[4,5]

In this work, we design a new D-A-D type of small-molecule OPV donors. Since there can be a plethora of possible combinations of D and A units, a virtual pre-synthesis screening would be mandatory for a rational design of small-molecule OPV donors. We have well described molecular orbital (MO) energy levels, bandgaps, UV/VIS absorption spectra, and PCE's of various D-A polymer donors with density functional theory (DFT) and time-dependent DFT (TDDFT) calculations at the B3LYP/6-311G(d,p) level on their short oligomer (~2 nm) models.[6-10] Contrary to a concern about the accuracy of the B3LYP functional in describing long-range charge transfer, this level of theory has been surprisingly suitable for studying OPV donor polymers. Our interpretation is that the charge transfer involved in OPV is rather short-range and the polymers are planar only over rather short (~2 nm) conjugation lengths. Since it could be also owing to a fortunate cancellation between the error from the B3LYP functional in describing long-range charge transfer and the error from the short oligomer model in representing polymers, it would be very interesting to see how well the same level of theory would describe the characteristics of small-molecule OPV donors.

Therefore we first validate our calculation method against the experiments on the best known components of small-molecule OPV cells, phenyl-C_{61}-butyric acid methyl ester ($PC_{61}BM$) acceptor and DTS(PTTh$_2$)$_2$ donor (**0**; Fig. 1).[1] We then use the same method to predict the (electronic) structure and PCE of new D-A-D-type small-molecule donors (**1**-**4**; Fig. 2) comprised of benzodithiophene (BDT; D) and thienopyrroledione (TPD; A) units. The BDT-TPD-BDT core, which mimics the [-BDT-TPD-]$_n$ copolymer donors employed in high-PCE (~8.5%) OPV cells,[11,12] is end-capped by self-assembly (SA) units which are expected to form a hydrogen-bonding network. Among the four units considered, pyridone is selected as the electronically best end-capping unit. The PCE of this combination **4**, however, is disappointingly low (~2%) due to the wide band gap, as confirmed experimentally. This is improved up to ~9% by varying the A unit from TPD to benzodiathiazole (BT) and its derivatives (**5**-**7**; Fig. 3).

[a] School of Materials Science and Engineering, Gwangju Institute of Science and Technology, Gwangju 61005, Korea.
[b] Research Institute for Solar and Sustainable Energies, Gwangju Institute of Science and Technology, Gwangju 61005, Korea
[c] Department of Chemistry, Gwangju Institute of Science and Technology, Gwangju 61005, Korea.
[d] GREMAN, UMR 7347, Université François Rabelais, 37200 Tours, France.
[*] Corresponding author: yhjang@gist.ac.kr, shong@gist.ac.kr, lansac@univ-tours.fr
[#] Electronic Supplementary Information (ESI) available: Detailed calculations (dihedral energy curves between units, Cartesian coordinates of optimized structures, and solvation effects) and experiment (methods and results). DOI: 10.1039/x0xx00000x.

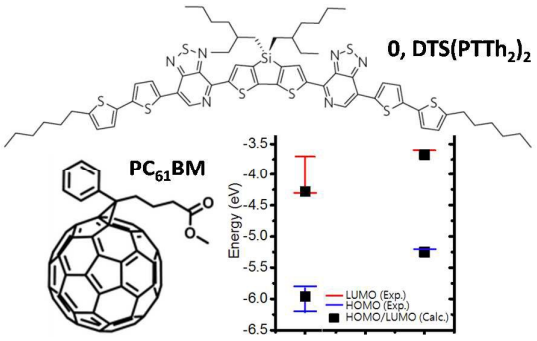

Fig. 1. Calculated (black mark) and measured (blue and red bars) E_{HOMO} and E_{LUMO} of PCBM and DTS(PTTh$_2$)$_2$ (**0**). See text in Section 3.1 for the references.

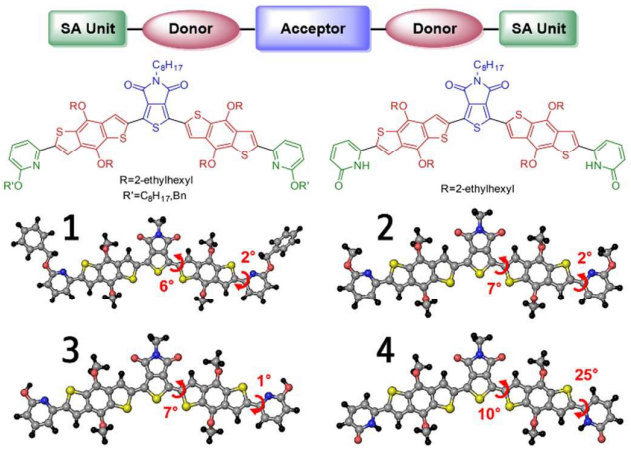

Fig. 2. D-A-D small-molecule donors **1**-**4** where BDT-TPD-BDT is end-capped by different SA units. **4** (pyridone) is a lower-energy tautomer of **3** (pyridinol). Alkyl side chains are replaced by methyl groups. Color code: black (H), gray (C), blue (N), red (O), yellow (S).

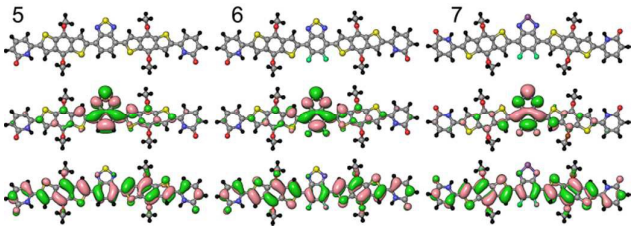

Fig. 3. Small-molecule donors **5**-**7** with BDT (D), pyridone (SA), and various A units (top) and their HOMO (middle) and LUMO (bottom). Color code: black (H); gray (C); blue (N); red (O); turquoise (F); yellow (S); wine (Se); green/pink (positive/negative MO phase).

2. Calculation Details

The same type of calculation is carried out as done in our previous studies.[6-10] The gas-phase ground-state geometry is fully optimized at the B3LYP/6-311G(d,p) level of DFT[13-17] using *Jaguar v6.5*.[18,19] Each component unit (SA, D, and A) is fully optimized, and then each pair of them (SA-D and D-A, that is, four different SA-BDT combinations as well as BDT-TPD) is connected at various dihedral angles and fully optimized. All the possible pairing combinations and their dihedral energy curves are shown in Fig. S1 of ESI. The lowest-energy pair conformers are connected to build the whole molecule **0**-**7** and fully optimized. All the alkyl side chains added to increase the solubility are replaced by methyl groups to simplify the calculations. The optimized geometries are confirmed to be the true minimum using the normal mode analysis, and the atomic Cartesian coordinates are given in Table S1-S9 of ESI. The energy levels of the highest occupied MO (HOMO), E_{HOMO}, are taken from the eigenvalues of the Kohn-Sham equation. In principle, the first ionization potential [IP = E(cation) – E(neutral)] should be more appropriate to compare with experimental E_{HOMO}, which is estimated electrochemically from the oxidation onset potential,[20] but inspection of previous studies including ours[6] indicates that our approach is rather simple and reliable. At each optimized geometry, the singlet-singlet electronic transition energies are calculated at the same level of theory using TDDFT[21-24] in *Gaussian09*.[25] The lowest ($S_0 \rightarrow S_1$) vertical transition energy gives the optical band gap (E_g; eV) corresponds to the lowest peak maximum λ_{max} (not the onset λ_{onset}) in the absorption spectrum (E_g = 1240 / λ_{max}; in nm). Our band gap E_g should be compared with literature with care, because the optical band gaps in literature (ref. 20, for example) are typically much lower values converted from the absorption onset wavelengths λ_{onset}. Since most (~98%) of the lowest-energy ($S_0 \rightarrow S_1$) transition comes from the transition from HOMO to the lowest unoccupied molecular orbitals (LUMO), the lowest TDDFT transition energy can be approximated as the HOMO-LUMO energy gap. The LUMO energy level, E_{LUMO}, is estimated by adding E_{HOMO} of DFT and the TDDFT transition energy [E_{LUMO} = E_{HOMO} (DFT) + E_g (TDDFT)]. Since the solvent effect of chloroform ($CHCl_3$) considered with the same implicit solvation model as done in our previous work[10] turns out to be marginal (ΔE_g < 30 nm or 0.08 eV; see ESI for details), we use the gas-phase calculations for the following discussion.

3. Results and discussion

3.1. Validation: PC$_{61}$BM and DTS(PTTh$_2$)$_2$. The E_{HOMO}, E_{LUMO}, and E_g values (in eV; Fig. 1) calculated for PC$_{61}$BM (-6.00, -4.25, and 1.75) and DTS(PTTh$_2$)$_2$ (**0**; -5.25, -3.67, and 1.59) are in good agreement with those measured electrochemically (CV) or optically (UV/vis): -5.80, -6.0, -6.10, -6.18, -6.2 (vs. -6.0), -3.70, -3.80, -3.95, -4.30 (vs. -4.25), and 1.7, 1.80, 2.00, 2.25, 2.48 (vs. 1.75) for PC$_{61}$BM[26-31] as well as -5.2 (vs. -5.25), -3.6 (vs. -3.67), and 1.6, 1.72, 1.89 (vs. 1.59) for **0**.[1] Our calculation appears to be reliable for predicting E_{HOMO} and the lower end of E_g of small-molecule donors. The agreement shown for polymeric donors in our past studies should be genuine with only a small amount of fortunate error cancellation.

The PCE of a PCBM-based BHJ OPV cell can be estimated from the E_g and E_{LUMO} values of the constituting donor using the Scharber diagram,[26,32,33] which has been constructed from the insight that a high PCE comes from a high open-circuit voltage V_{OC} (a driving force for exciton dissociation; $\propto E_{LUMO}$[acceptor] - E_{HOMO}[donor] - 0.3 eV), a high short-circuit current J_{SC} ($\propto$ solar spectrum integrated above E_g[donor]), and a high fill factor FF (fixed as 0.65). A prerequisite of using the Scharber diagram for the PCE prediction is that the hole mobility of the donor should be higher than 10^{-3} cm^{2}V^{-1}s^{-1} to ensure FF higher than 0.65.[26,32,33] The hole mobility of DTS(PTTh$_2$)$_2$ (**0**) has been reported[1] as 6×10^{-3} cm^{2}V^{-1}s^{-1}, satisfying the prerequisite. Plugging E_g (1.59 eV) and E_{LUMO} (-3.67 eV) calculated for **0** into the Scharber diagram predicts that **0** would show a PCE up to 7% (blue dot, Fig. 4), and this indeed agrees with 6.7% measured with a morphology control using 1,8-diiodooctane (DIO) additives.[1]

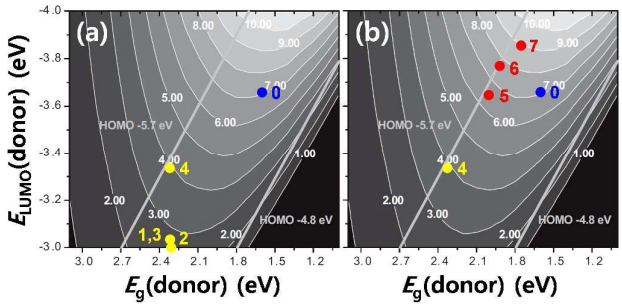

Fig. 4. Scharber diagram to estimate PCE (in %) for **0** (blue), **1**-**4** (yellow) and **5**-**7** (red), which is adapted from the work of Scharber and coworkers[26,32] with permission from Wiley-VCH

3.2. Varying SA: 1-4. Now the same type of calculation is carried out on new D-A-D (BDT-TPD-BDT) small-molecule donors which are end-capped with four different SA (pyridinol-derivative) units (**1**-**4**, Fig. 2). Only **4** is significantly (25°) twisted around pyridone (low-energy tautomer of pyridinol) termini in its minimum-energy conformation, and all the others (**1**-**3**) with pyridinol-derivative termini have a nearly planar (<10°) minimum-energy structure with a significant (6 kcal/mol) torsion barrier (as shown in the dihedral energy curves between the component units; Fig. S1 in ESI). The overall planarity of **1**-**4** would give a high degree of π-conjugation and low E_g. The predicted frontier MO energy diagram of **1**-**4** (in eV) is shown in Fig. 5. E_{HOMO} is calculated as -5.33, -5.30, -5.35, and -5.67, E_g as 2.31, 2.31, 2.32, and 2.34 (equivalently, λ_{max} as 537, 537, 535, and 530 nm), and thus E_{LUMO} as -3.02, -2.99, -3.04, and -3.33. E_{HOMO} and E_{LUMO} are significantly (by 0.3 eV) lower for **4** than for the others, but E_g is essentially the same for **1**-**4** (2.31-2.34 eV). Contrary to their polymer analogues, this series of small-molecule donors have too wide E_g (2.31-2.34 eV corresponding to λ_{max} of 530-537 nm) to absorb the near-IR solar spectrum of 680-950 nm.

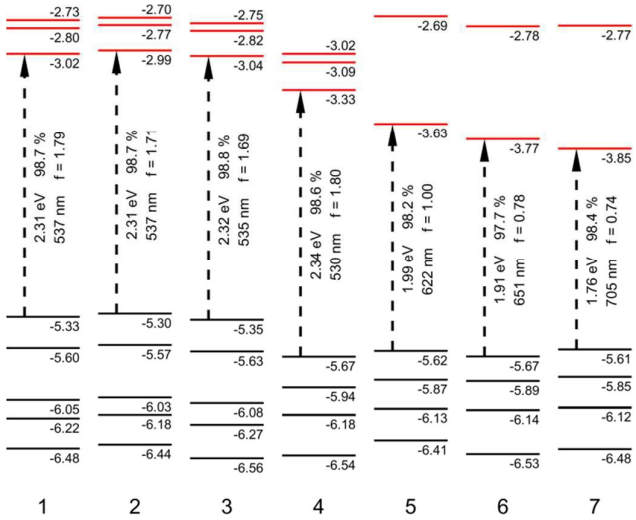

Fig. 5. Predicted frontier MO energy diagram (in eV) of **1**-**7** which shows several HOMO (black bar) and LUMO (red bar) levels of each compound as well as the lowest-energy ($S_0 \rightarrow S_1$) electronic transition (black dashed vertical arrow; in eV and nm), the oscillator strength (*f*), and the contribution from the HOMO-to-LUMO transition.

The Scharber diagram (yellow dots, Fig. 4a) predicts that, among the compounds **1**-**4** which exhibit essentially the same E_g (2.31-2.34 eV), the compound **4** with the lowest E_{LUMO} (-3.33 eV) would show the highest PCE up to 4% while the other compounds **1**-**3** with E_{LUMO} around -3.0 eV would show PCE less than 2.7%, assuming that they would also satisfy the prerequisite of sufficiently high hole mobility for the Scharber-diagram-based PCE prediction.

3.3. Validation Experiments with Synthetic Compound 1. To confirm the predicted MO energy levels and PCE as well as the required hole mobility, we first synthesize the compound **1** having a benzyloxy group on the pyridine as SA (BnOPy-BDT-TPD-BDT-PyOBn; Synthesis of the other compounds **2**-**4** has not been successful so far) and fabricate its devices (see ESI for the experimental details).

The E_g and E_{HOMO} are measured with UV/VIS spectroscopy and cyclic voltammetry (CV). Fig. 6a shows that the spectroscopic data from the UV/VIS measurement on a thin film of **1** (λ_{max} 555 nm, E_g 2.23 eV, λ_{onset} 614 nm, and E_g^{opt} 2.02 eV; black curve) and on **1** in chloroform solution (λ_{max} 505 nm and E_g 2.46 eV; blue curve) are in agreement with the TDDFT calculation (λ_{max} 537 nm and E_g 2.31 eV; red vertical line). Furthermore, Fig. 6b shows that the E_{HOMO} of **1** is estimated as -5.26 eV (E_{HOMO} = - E_{onset} - 4.8 eV)[34] from the onset oxidation potential (E_{onset} 0.86 V) measured in the CV experiments, and this agrees well with -5.33 eV from the DFT calculation.

Then, its inverted solar cells (ITO/ZnO/**1**:$PC_{70}BM$/MoO_3/Ag) are fabricated with and without a morphology control using DIO additives, and their photovoltaic performances are evaluated from the current density-voltage (*J*-*V*) curves (Fig. 6c) as 0.80 and 0.82 V (V_{OC}), 4.53 and 4.48 mA/cm^2 (J_{SC}), 0.46 and 0.44 (FF), as well as 1.7% and 1.6% (PCE = $V_{OC} \times J_{SC} \times$ FF), respectively. The large E_g of **1** leads to a narrow external quantum efficiency (EQE) absorption spectrum (Fig. 6d, 300-700 nm rather than 300-800 nm of **0**)[1] and its disrupted molecular orientation and connection in BHJ domains limits the EQE (Fig. 6d, up to 35% rather than 68% of **0**),[1] resulting in relatively low photocurrents J_{SC}.

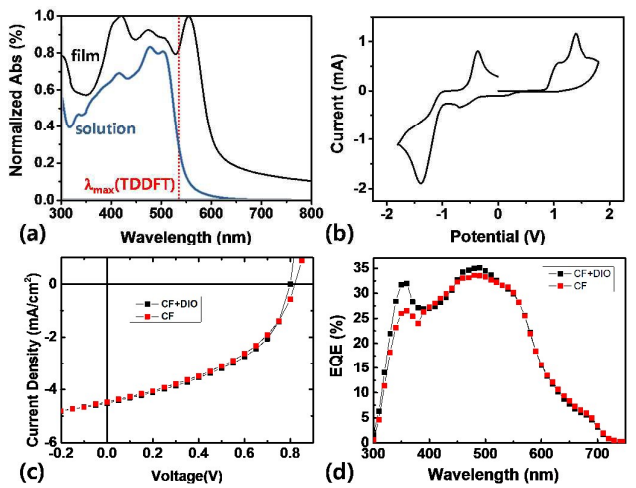

Fig. 6. Experimental data for **1**, PyOBn-BDT-TPD-BDT-PyOBn. (a) UV/VIS spectra in $CHCl_3$ (CF) solution (blue) and thin film (black) shown with the peak maximum position predicted by TDDFT (red), (b) CV, (c) *J*-*V* curves, and (d) external quantum efficiency spectra taken with and without 1,8-diiodooctane (DIO) additives.

The hole mobility of **1** measured in organic field effect transistors fabricated on octadecyltrichlorosilane-treated SiO_2/Si substrates with Ag source and drain electrodes is 1.1×10^{-3} $cm^2V^{-1}s^{-1}$ (much lower than 0.12 of **0**),[1] resulting in FF as low as 0.44 (much lower than 0.59 of **0**).[1] Therefore the maximum PCE measured for **1** (1.7%) is much lower than 6.7% measured for **0**.[1] It is also significantly lower than 2.7% predicted for **1** (Fig. 4a), most likely because the hole mobility (1.1×10^{-3} $cm^2V^{-1}s^{-1}$) barely satisfies the prerequisite ($>10^{-3}$ $cm^2V^{-1}s^{-1}$) of the Scharber diagram and the FF (0.44) is still significantly lower than its assumption (0.65) without improvement after adding DIO, on the contrary to the substantial improvement achieved for **0** (0.45 to 0.59).[1] Considering the difference in the end-capping unit between **0** (long alkyl chain) and **1** (aromatic SA unit), we believe that the morphology of **1** could be further improved either by adding long alkyl chains to the SA units of **1** or by devising a better way (than adding DIO) to induce hydrogen-bonding self-assembly networks via the SA units of **1**, so that the experimental hole mobility, FF, and in turn PCE (currently 1.7%) would be further improved approaching the upper limit of PCE (2.7%) predicted by intrinsic electronic structure calculations (which could be adjusted by simulations of BHV morphology and charge transfer/transport hopefully in near future).

3.4. Varying A: 5-7. In fact, not only **1** but also the whole series **1**-**4** are predicted to have low PCE (2.5-4%) due to their consistently wide E_g (~2.3 eV). The E_g of this series is controlled by the D-A-D core rather than the SA unit (see the four yellow dots vertically aligning in Fig. 4a whose x-axis denotes E_g). This is explained by the relative positions of E_{HOMO} (pink) and E_{LUMO} (green) of the pyridone (SA), BDT (D), and TPD (A) component units shown in Fig. 7 (three columns on the left). The highest E_{HOMO} and the lowest E_{LUMO} among them would determine the E_{HOMO} and the E_{LUMO} of their composites, respectively. Therefore, the E_{HOMO} and E_{LUMO} of **1**-**4** are determined mostly by the E_{HOMO} of the D unit (BDT) and the E_{LUMO} of the A unit (TPD), respectively, while the SA unit makes only an inductive effect to shift up and down the E_{HOMO} and E_{LUMO} together (see again the four yellow dots vertically distributing in Fig. 4a whose y-axis shows E_{LUMO}). Therefore, enhancing PCE by reducing E_g could be difficult if we keep the BDT-TPD-BDT core.

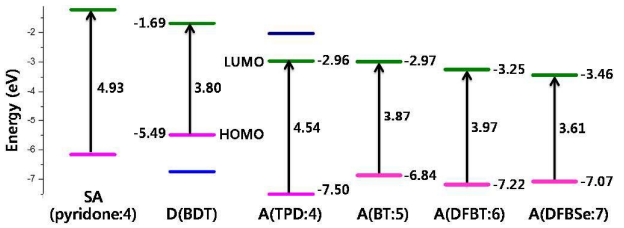

Fig. 7. Frontier MO energy diagrams (HOMO in pink and LUMO in green) of the SA (fixed as pyridone), D (fixed as BDT), and A (varied from TDP to BT and its derivatives) component units for **4**-**7** donors.

Instead, since E_{HOMO} of **4** (-5.67 eV) is sufficiently low, we decide to modify **4** in a direction to lower E_{LUMO} (and accordingly E_g) while keeping E_{HOMO} intact, that is, to follow up the white line starting from the yellow dot of **4** in Fig. 6. This would be realized by altering the A unit,[35,36] while keeping the D unit as BDT and the SA unit as pyridone. On the basis of E_{LUMO} compared in Fig. 7 (four columns on the right), we choose three A units having lower E_{LUMO} than TPD to virtually build a new series of small-molecule donors where the A unit of **4** (TPD) is replaced by benzothiadiazole (BT; **5**), 5,6-difluoro-BT (DFBT; **6**), and 5,6-difluorobenzoselenadiazole (DFBSe; **7**) (Fig. 3).

The frontier MO distributions and energy diagram (in eV) of **5**-**7** are shown in Figs. 3 and 5. Indeed, we see in Fig. 3 that the HOMO and LUMO of **5**-**7** are distributed on the D and A units, respectively, and in Fig. 5 that the low E_{HOMO} of **4** (-5.67) is kept intact in **5** (-5.62), **6** (-5.67), and **7** (-5.61) while E_{LUMO} is significantly lower in **5** (-3.63), **6** (-3.77), and **7** (-3.85) than in **4** (-3.33). Accordingly, E_g is narrower in **5** (1.99), **6** (1.91), and **7** (1.76) than in **4** (2.34), and equivalently λ_{max} (in nm) is longer in **5** (622), **6** (651), and **7** (705) than in **4** (530). This new series **5**-**7**, particularly **6**-**7**, would be able to absorb the near-IR region (680-950 nm) of the solar spectrum. Indeed, the Scharber diagram predicts that the PCBM-based BHJ OPV cells made of **5**-**7** (red dots, Fig. 4b) would show significantly higher PCEs than those made of **1**-**4** [**1**-**3** (2.7%) << **4** (4%) << **5** (6.5%) < **6** (7.8%) < **7** (9%)] under the condition that they would show a high hole mobility ($>10^{-3}$ $cm^2V^{-1}s^{-1}$) and FF (~0.65). The dihedral energy curves calculated for **5**-**7** (not shown) indicate that the nearly planar conformation of **1**-**4** would be kept in **5**-**7** having the minimum-energy dihedral angle less than 10°, and thus the intermolecular π-π stacking favorable for structural organization and morphology control would be still eligible in this new series. We thus propose **5**-**7** as *electronically* promising candidates to be used as a small-molecule donor in PCBM-based BHJ OPV cells, although their synthesis has not been successful so far and a new strategy still needs to be developed to improve their morphology. If such issues in synthesis, morphology, and BHJ-electrode contact could be successfully solved, they have a potential to reach 6-9% of PCE.

4. Conclusions

Our DFT/TDDFT (B3LYP/6-311G**) calculations on both molecular and polymeric OPV donors well reproduce their frontier MO energy levels observed in experiments. Among newly-proposed D-A-D-type small-molecule donors **1**-**4** end-capped by different SA units, **4** end-capped by pyridone units is predicted to have the highest PCE (4% ideally) owing to its relatively low HOMO and LUMO energy levels. Further enhancement of PCE (to 6-9% ideally) is achieved with **5**-**7**, which are rationally-designed from **4** by altering the A unit in the direction lowering the band gap and the LUMO energy level while keeping the HOMO energy level. Synthesis of promising candidates would be highly interesting and is currently in progress.

Acknowledgements

This work was supported by the Korean CCS 2020 Program (2014M1A8A1049267, 2014M1A8A1049321), the Basic Research Program (2013R1A1A3012254), and the Global Frontier Hybrid Interface Materials Program (2013M3A6B1078882) of the Korean National Research Foundation, by the Brain Pool Program (151S-1-3-1232) of KOFST, and by the Grand Challenge (KSC-2014-C3-032) and PLSI programs of KISTI. S.H. thanks support by the Core Technology Development Program for Next-Generation Solar Cells of Research Institute for Solar and Sustainable Energies (RISE), GIST.

Notes and references

1 Y. Sun, G. C. Welch, W. L. Leong, C. J. Takacs, G. C. Bazan and A. J. Heeger, Nat. Mater., 2012, 11, 44.
2 J. Roncali, P. Frere, P. Blanchard, R. de Bettignies, M. Turbiez, S. Roquet, P. Leriche and Y. Nicolas, Thin Solid Films, 2006, 511-512, 567.
3 X. Sun, Y. Zhou, W. C. Wu, Y. Liu, W. Tian, G. Yu, W. Qiu, S. Chen and D. Zhu, J. Phys. Chem. B, 2006, 110, 7702.
4 J. Zhou, Y. Zuo, X. Wan, G. Long, Q. Zhang, W. Ni, Y. Liu, Z. Li, G. He, L. C., B. Kan, M. Li and Y. Chen, J. Am. Chem. Soc., 2013, 135, 8484.
5 Q. Zhang, B. Kan, F. Liu, G. Long, X. Wan, X. Chen, Y. Zuo, W. Ni, H. Zhang, M. Li, Z. Hu, F. Huang, Y. Cao, Z. Liang, M. Zhang, T. P. Russell and Y. Chen, Nat. Photonics, 2015, 9, 35.
6 J. Ku, Y. Lansac and Y. H. Jang, J. Phys. Chem. C, 2011, 115, 21508.
7 J. Ku, D. Kim, T. Ryu, E. Jung, Y. Lansac and Y. H. Jang, Bull. Korean Chem. Soc., 2012, 33, 1029.
8 N. I. Abdo, J. Ku, A. A. El-Shehawy, H.-S. Shim, J.-K. Min, A. A. El-Barbary, Y. H. Jang and J.-K. Lee, J. Mater. Chem. A, 2013, 1, 10306.
9 J. Ku, S. Song, S. H. Park, K. Lee, H. Suh, Y. Lansac and Y. H. Jang, J. Phys. Chem. C, 2015, 119, 14063.
10 J. Ku, Y. Gim, Y. Lansac and Y. H. Jang, Phys. Chem. Chem. Phys., 2016, 18, 1017.
11 C. Cabanetos, A. El Labban, J. A. Bartelt, J. D. Douglas, W. R. Mateker, J. M. J. Fréchet, M. D. McGehee and P. M. Beaujuge, J. Am. Chem. Soc., 2013, 135, 4656.
12 W. R. Mateker, J. D. Douglas, C. Cabanetos, I. T. Sachs-Quintana, J. A. Bartelt, E. T. Hoke, A. El Labban, P. M. Beaujuge, J. M. J. Fréchet and M. D. McGehee, Energy Environ. Sci., 2013, 6, 2529.
13 J. C. Slater, Quantum Theory of Molecules and Solids. Vol. 4. The Self-Consistent Field for Molecules and Solids, McGraw-Hill, New York, 1974.
14 A. D. Becke, Phys. Rev. A, 1988, 38, 3098.
15 S. H. Vosko, L. Wilk and M. Nusair, Can. J. Phys., 1980, 58, 1200.
16 C. Lee, W. Yang and R. G. Parr, Phys. Rev. B, 1988, 37, 785.
17 B. Miehlich, A. Savin, H. Stoll and H. Preuss, Chem. Phys. Lett., 1989, 157, 200.
18 Schrodinger, LLC, New York, NY, version 6.5 edn., 2005.
19 B. H. Greeley, T. V. Russo, D. T. Mainz, R. A. Friesner, J.-M. Langlois, W. A. Goddard, III, R. E. Donnelly, Jr. and M. N. Ringalda, J. Chem. Phys., 1994, 101, 4028.
20 L. Pandey, C. Risko, J. E. Norton and J.-L. Brédas, Macromolecules, 2012, 45, 6405.
21 E. Runge and E. K. U. Gross, Phys. Rev. Lett., 1984, 52, 997.
22 R. E. Stratmann, G. E. Scuseria and M. J. Frisch, J. Chem. Phys., 1998, 109, 8218.
23 M. E. Casida, C. Jamorski, K. C. Casida and D. R. Salahub, J. Chem. Phys., 1998, 108, 4439.
24 K. Burke, J. Werschnik and E. K. U. Gross, J. Chem. Phys., 2005, 123, 062206.
25 M. J. Frisch, G. W. Trucks, H. B. Schlegel, G. E. Scuseria, M. A. Robb, F. R. Cheeseman, J. A. F. Montgomery, T. Vreven, K. N. Kudin, J. C. Burant, F. M. Millam, S. S. Iyengar, F. Tomasi, V. Barone, B. Mennucci, M. Cossi, G. Scalmani, N. Rega, G. A. Petersson, G. Nakatsufi, M. Hada, M. Ehara, K. Toyota, R. Fukuda, J. Hasegawa, M. Ishida, T. Nakajima, Y. Honda, O. Kitao, G. Nakai, M. Klene, X. Li, J. E. Know, G. P. Hratchian, J. B. Cross, V. Bakken, C. Adamo, F. Jaramillo, R. Gomperts, R. E. Stratmann, O. Yazyev, A. J. Austin, R. Cmmi, C. Pomelli, J. W. Ochterski, P. Y. Ayala, K. Morokuma, G. A. Voth, P. Salvador, J. J. Dnnenberg, V. G. Zakrzewski, S. Dapprich, A. D. Daniels, M. C. Strain, O. Farkas, D. K. Malick, A. D. Rabuck, R. K., J. B. Foresman, J. V. Ortiz, Q. Cui, A. G. Baboul, S. Clifoord, J. Coislowski, B. B. Stefanov, G. Liu, A. liashenko, P. Piskorz, I. Komaromi, R. L. Martin, D. J. Fox, T. Keith, M. A. Al-Laham, C. Y. Peng, A. Nanayakkara, M. Challacombe, P. M. W. Gill, B. Jognson, W. Chen, M. W. Wong, C. Gonzalez and J. A. Pople, Gaussian, Inc., Wallingford, CT, Revision C.02 edn., 2004.
26 M. C. Scharber, D. Muhlbacher, M. Koppe, P. Denk, C. Waldauf, A. J. Heeger and C. J. Brabec, Adv. Mater., 2006, 18, 789.
27 J. Y. Kim, K. Lee, N. E. Coates, D. Moses, T.-Q. Nguyen, M. Dante and A. J. Heeger, Science, 2007, 317, 222.
28 H.-Y. Chen, J. Hou, S. Zhang, Y. Liang, G. Yang, Y. Yang, L. Yu, Y. Wu and G. Li, Nature Photon., 2009, 3, 649.
29 Z.-L. Guan, J. B. Kim, H. Wang, C. Jaye, D. A. Fischer, Y.-L. Loo and A. Kahn, Org. Electron., 2010, 11, 1779.
30 J. A. Mikroyannidis, A. N. Kabanakis, S. S. Sharma and G. D. Sharma, Adv. Funct. Mater., 2011, 21, 746.
31 S. H. Yoo, J. M. Kum and S. O. Cho, Nanoscale Res. Lett., 2011, 6, 545.
32 N. Blouin, A. Michaud, D. Gendron, S. Wakim, E. Blair, R. Neagu-Plesu, M. Belletete, G. Durocher, Y. Tao and M. Leclerc, J. Am. Chem. Soc., 2008, 130, 732.
33 N. Berube, V. Gosselin, J. Gaudreau and M. Cote, J. Phys. Chem. C, 2013, 117, 7964.
34 C. M. Cardona, W. Li, A. E. Kaifer, D. Stockdale and G. C. Bazan, Adv. Mater., 2011, 23, 2367.
35 H. Zhong, Z. Li, E. Buchaca-Domingo, S. Rossbauer, S. E. Watkins, N. Stingelin, T. D. Anthopoulos and M. Heeney, J. Mater. Chem. A, 2013, 1, 14973.
36 A. Casey, Y. Han, Z. Fei, A. J. P. White, T. D. Anthopoulos and M. Heeney, J. Mater. Chem. C, 2015, 3, 265.